

Consequences of the General Corrosion of Carbon Steel Used Fuel Containers for Gas Generation in a DGR

NWMO TR-2013-16

December 2013

Fraser King

Integrity Corrosion Consulting Ltd.

nwmo

NUCLEAR WASTE
MANAGEMENT
ORGANIZATION

SOCIÉTÉ DE GESTION
DES DÉCHETS
NUCLÉAIRES



Nuclear Waste Management Organization
22 St. Clair Avenue East, 6th Floor
Toronto, Ontario
M4T 2S3
Canada

Tel: 416-934-9814
Web: www.nwmo.ca

Consequences of the General Corrosion of Carbon Steel Used Fuel Containers for Gas Generation in a DGR

NWMO TR-2013-16

December 2013

Fraser King
Integrity Corrosion Consulting Ltd.

This report has been prepared under contract to NWMO. The report has been reviewed by NWMO, but the views and conclusions are those of the authors and do not necessarily represent those of the NWMO.

All copyright and intellectual property rights belong to NWMO.

Document History

Title:	Consequences of the General Corrosion of Carbon Steel Used Fuel Containers for Gas Generation in a DGR		
Report Number:	NWMO TR-2013-16		
Revision:	R000	Date:	December 2013
Author Company(s)			
Authored by:	Fraser King, Integrity Corrosion Consulting Ltd.		
Reviewed by:	Jamie Noël, Jamie Noël Consulting		
Nuclear Waste Management Organization			
Reviewed by:	Peter Keech, Sr. Scientist, Container Corrosion and Coatings		
Reviewed by:	Erik Kremer, Sr. Engineer/Scientist		
Reviewed by:	David Doyle, Manager Used Fuel Container Development		
Accepted by:	Chris Hatton, Director Repository Design and Development		

ABSTRACT

Title: Consequences of the General Corrosion of Carbon Steel Used Fuel Containers for Gas Generation in a DGR
Report No.: NWMO TR-2013-16
Author: Fraser King
Company: Integrity Corrosion Consulting Ltd.
Date: December 2013

Abstract

The general corrosion of carbon steel (C-steel) containers in a deep geologic repository will result in both the consumption and generation of gaseous species. Under aerobic conditions, corrosion will lead to the consumption of O₂, either due to gas-phase oxidation or subsequent corrosion in a thin surface moisture film under unsaturated conditions. Once the O₂ has been consumed, the anaerobic corrosion of C-steel will result in the generation of H₂ and the possible formation of a gaseous hydrogen phase.

A critical review of the corrosion rates of C-steel under conditions relevant to those expected in the repository has been performed, with recommendations given for best-estimate corrosion rates. For the purposes of the review, the evolution of the environmental conditions in the repository has been divided into four phases:

- Phase 1 A period during the initial thermal transient when the relative humidity in the repository is below that necessary for the formation of liquid H₂O on the container surface. Corrosion during this phase will be limited to slow air oxidation.
- Phase 2: An early phase of unsaturated aerobic conditions prior to saturation of the repository and during which corrosion is supported by the reduction of the O₂ trapped initially in the pores of the buffer and backfill materials.
- Phase 3: An intermediate unsaturated anaerobic phase following the consumption of the O₂ but prior to the saturation of the repository. Corrosion during this period is supported by the cathodic reduction of H₂O accompanied by the evolution of H₂.
- Phase 4: A long-term saturated anaerobic period following saturation of the repository. As for Phase 3, corrosion during Phase 4 is supported by the cathodic reduction of H₂O accompanied by the evolution of H₂.

The rate of oxidation of C-steel in dry air (Phase 1) is low at the temperatures of interest (i.e. below 120°C) and will result in a few µm of corrosion. Although the rate of aerobic corrosion in the presence of moisture under unsaturated conditions (Phase 2) is higher, the extent of corrosion is limited by the initial inventory of trapped O₂ in the repository. Therefore, following the establishment of aqueous conditions, the duration of aerobic corrosion is predicted to be less than 1 a.

Of most interest is the rate of anaerobic corrosion under first unsaturated (Phase 3) and subsequently saturated (Phase 4) conditions. Based on the review of literature corrosion studies, these rates are temperature dependent, with the rate decreasing with time as the container surface cools.

Recommended corrosion rate expressions are given for each of the four phases.

TABLE OF CONTENTS

	<u>Page</u>
ABSTRACT	iii
1. INTRODUCTION.....	1
2. ENVIRONMENTAL CONDITIONS.....	2
3. REVIEW OF CORROSION INFORMATION.....	6
3.1 DRY AIR OXIDATION.....	6
3.2 AEROBIC UNSATURATED CONDITIONS.....	7
3.3 ANAEROBIC UNSATURATED CONDITIONS.....	10
3.4 ANAEROBIC SATURATED CONDITIONS.....	14
3.5 TRANSITION BETWEEN PHASES.....	16
4. RECOMMENDED CORROSION RATE DATA.....	17
4.1 PHASE 1 DRY AIR OXIDATION.....	17
4.2 PHASE 2 AEROBIC UNSATURATED CONDITIONS.....	18
4.3 PHASE 3 ANAEROBIC UNSATURATED CONDITIONS.....	20
4.4 PHASE 4 ANAEROBIC SATURATED CONDITIONS.....	21
5. UNCERTAINTIES AND CONFIDENCE.....	23
REFERENCES	25

LIST OF FIGURES

	<u>Page</u>
Figure 1: The Deliquescence Behaviour of Commonly Observed Salt Contaminants.....	3
Figure 2: Suction Potential of MX80 Bentonite as a Function of the Degree of Saturation and Buffer Density (Man and Martino 2009).....	4
Figure 3: Dependence of the Suction Potential and Relative Humidity on the Degree of Saturation for Highly Compacted Bentonite Based on Equations (1) and (3), Respectively.	5
Figure 4: The Effect of Temperature on the Aerobic Corrosion Rate of Steel in Humid Air, Bulk Solution, and in the Presence of Backfill Material.	8
Figure 5: Arrhenius Plot of the Aerobic Corrosion Rate Data from Figure 4.	9
Figure 6: Effect of Temperature on the Time Dependence of the Corrosion Rate of Carbon Steel Under Anaerobic Conditions at 100% Relative Humidity Following Pre-corrosion in 0.5 mol·dm ⁻³ NaCl Solution (Newman et al. 2010).	11
Figure 7: Arrhenius Plot of the Anaerobic Corrosion Rate of Carbon Steel at 100% Relative Humidity.....	11
Figure 8: Effect of Relative Humidity on the Time Dependence of the Corrosion Rate of Carbon Steel Under Anaerobic Conditions at 32°C Following Pre-corrosion in 0.5 mol·dm ⁻³ NaCl Solution (Newman et al. 2010).	12
Figure 9: Effect of Relative Humidity on the Time Dependence of the Corrosion Rate of Carbon Steel Under Anaerobic Conditions at 50°C Following Pre-corrosion in 0.5 mol·dm ⁻³ NaCl Solution (Newman et al. 2010).	13
Figure 10: Summary of Differences Between the Anaerobic Corrosion Behaviour of Carbon Steel in Bulk Solution and in Compacted Clay (Johnson and King 2008, King 2008).	14
Figure 11: Temperature Dependence of the Corrosion Rate of Carbon Steel in Compacted Clay. Tests with exposure periods of 12 months or less are shown as filled symbols, with results from longer tests shown as open symbols.	15
Figure 12: Arrhenius Plot of the Temperature Dependence of the Corrosion Rate of Carbon Steel in Compacted Clay Based on the Data in Figure 11. Also shown on the figure is a proposed dependence by Gras (1996).	16
Figure 13: Proposed Corrosion Rate Expressions for the Aerobic Unsaturated Period Compared with Measured Corrosion Rates in Aerated Solution and Humid Air.	19
Figure 14: Proposed Best-estimate and Upper and Lower Bound Corrosion Rate Fits for the Corrosion Rate of Carbon Steel During Phase 4.	22
Figure 15: Compilation of Corrosion Rates of Iron and Steel Exposed to Soils and Natural Waters (Crossland 2005).	24

1. INTRODUCTION

Corrosion of carbon steel (C-steel) used fuel containers (UFC) has a number of impacts on the performance of the repository system. First, corrosion in its various forms is the major contributing factor to container failure (King 2007), following which the release of radionuclides to the near field becomes possible. Second, dissolved ferrous species can interact with bentonite and convert swelling smectite clays to non-swelling illitic forms, resulting in a partial loss of swelling capacity (Wersin et al. 2007). Third, anaerobic corrosion will result in the generation of hydrogen which may form a gaseous H₂ phase in the repository, the presence of which could impact the migration of radionuclides. The current analysis is focussed primarily on the estimation of the rate of H₂ generation due to corrosion of the container.

The corrosion behaviour of the container will change with time as the environment in the repository evolves. From a corrosion perspective, the most important environmental factors are the UFC temperature, the redox conditions, the degree of saturation of the buffer material, and the composition of the bentonite pore water in contact with the UFC. For a deep geological repository (DGR) in low-permeability sedimentary host rock, saturation of the DGR may take tens of thousands of years. This slow saturation has led to the definition of four distinct phases in the evolution of the environment, namely: an early aerobic period prior to the onset of aqueous corrosion, a subsequent unsaturated aerobic phase following the condensation of liquid water on the container surface, an unsaturated anaerobic phase once all of the initially trapped O₂ has been consumed and, finally, a long-term saturated anaerobic phase once the buffer material has become completely saturated by ground water.

Hydrogen is produced by the cathodic reduction of H₂O or H⁺. The vast majority of H₂ that will be produced in the repository will result from the general corrosion of C-steel during the (unsaturated and saturated) anaerobic phase. Hydrogen can be produced under aerobic conditions due to the reduction of H⁺ in acidic environments in pits, crevices, or porous corrosion products formed as a result of the hydrolysis of Fe(III) species (Akiyama et al. 2010, Tsuru et al. 2005). Local reduction of H⁺ may lead to enhanced hydrogen absorption and environmentally assisted cracking (King 2009), but will not lead to the generation of significant H₂ and is not considered further here.

Hydrogen generated by corrosion can undergo a number of subsequent processes. The H₂ that is evolved could be consumed by microbes (Pedersen 2000) in those parts of the near- and far-fields in which the environment is conducive to microbial activity (namely a water activity greater than 0.95, Stroes-Gascoyne et al. 2006, 2007, 2008). Another fraction of the hydrogen will be absorbed by the C-steel as atomic H, either from adsorbed H atoms prior to their evolution as H₂ or via the dissociative absorption of gaseous H₂. Absorbed H will diffuse through the container wall and desorb on the inner surface as H₂ gas. This process will continue until the H₂ partial pressure inside the container is the same as that outside. Thus, the container acts as a sink for a fraction of the H produced through anaerobic corrosion.

The amount of this "immobilised" hydrogen is not insignificant. The H is present as absorbed H atoms in the canister wall and gaseous H₂ inside the container. The total absorbed H concentration for C-steel in solutions similar to bentonite pore water is of the order of 1 µg.g⁻¹ (King 2009). By way of illustration, the mass of the internal IV-25 steel vessel of the copper-steel UFC design (which would be similar to the design of an all-steel container) is 12.65 Mg (SNC Lavalin 2011), resulting in the absorption of the equivalent of 6.3 mol H₂. The internal void volume inside the container is 1.58 m³ (Garisto et al. 2012). Let us assume that a H₂ gas

phase forms in the buffer material at some stage during the repository evolution and that the maximum H₂ pressure is 8 MPa (King 2009). Once the internal H₂ partial pressure has reached this value, a process that could take from a few hundred to a few thousand years (Turnbull 2009), the internal void space would be filled with 5100 mol H₂ at 25°C, for a total quantity of immobilised H₂ of ~5110 mol. This amount of H₂ is equivalent to the anaerobic corrosion of 1.8 mm of the container wall (UFC surface area 15.4 m²), assuming the final corrosion product is Fe₃O₄.

The remainder of this technical memorandum deals with the rate of generation of H₂, rather than its fate in the repository. The environmental conditions in the repository are first considered, with emphasis on those conditions that affect the rate of corrosion (H₂ generation). Next, the general corrosion behaviour of C-steel for each of the four main phases in the evolution of the repository environment is reviewed, with some discussion of the transition between the various phases. Finally, recommendations are provided for corrosion rate expressions for each phase, along with a discussion of the confidence in these values.

2. ENVIRONMENTAL CONDITIONS

The environment in the repository will evolve with time as (i) the initially trapped O₂ is consumed, (ii) the heat output from the container decays, and (iii) the repository saturates with incoming ground water. The latter effect may be particularly important for a repository in sedimentary rock of low hydraulic conductivity as it may take tens of thousands of years for the DGR to saturate.

The corrosion behaviour of the container will also change with time in response to this environmental evolution. A series of four phases of corrosion behaviour can be defined, namely:

- Phase 1 A period during the initial thermal transient when the relative humidity in the repository is below that necessary for the formation of liquid H₂O on the container surface. Corrosion during this phase will be limited to slow air oxidation.
- Phase 2: An early phase of unsaturated aerobic conditions prior to saturation of the repository and during which corrosion is supported by the reduction of the O₂ trapped initially in the pores of the buffer and backfill materials.
- Phase 3: An intermediate unsaturated anaerobic phase following the consumption of the O₂ but prior to the saturation of the repository. Corrosion during this period is supported by the cathodic reduction of H₂O accompanied by the evolution of H₂.
- Phase 4: A long-term saturated anaerobic period following saturation of the repository. As for Phase 3, corrosion during Phase 4 is supported by the cathodic reduction of H₂O accompanied by the evolution of H₂.

In addition to the evolution of the redox conditions and the degree of saturation, the temperature will also change during these different phases. The precise time dependence of the container temperature will depend on the rate of saturation which is not known *ab initio*. However, in general, it is clear that Phases 1 and 2 will be warmer than Phase 3 and Phase 4.

The onset of aqueous corrosion (i.e., the transition from Phase 1 to Phase 2) is dependent on the relative humidity (RH) at the container surface. Aqueous corrosion is possible above a critical or threshold RH that is determined by the nature of the surface and the presence of surface contaminants. Water condenses on porous surfaces or corrosion products by capillary condensation. Salts absorb moisture from the atmosphere in a process known as deliquescence at a critical deliquescence RH (DRH) that is a function of temperature and the type of salt. Salts that are highly soluble deliquesce at lower RH than sparingly soluble salts. Figure 1 shows the DRH as a function of temperature for a number of salts and for one salt mixture. Highly deliquescent salts, such as $\text{CaCl}_2 \cdot x\text{H}_2\text{O}$ or MgCl_2 (not shown), will deliquesce at low humidity. Less-soluble salts, such as NaCl , deliquesce at higher RH. The commonly accepted threshold RH for the onset of atmospheric corrosion of 60-80% RH is consistent with the deliquescence behaviour of NaCl , a commonly observed surface salt contaminant. Mixed salts, such as those that might form from the evaporation of a complex ground or pore water solution, will deliquesce at a lower RH than those for the pure salts (Yang et al. 2001).

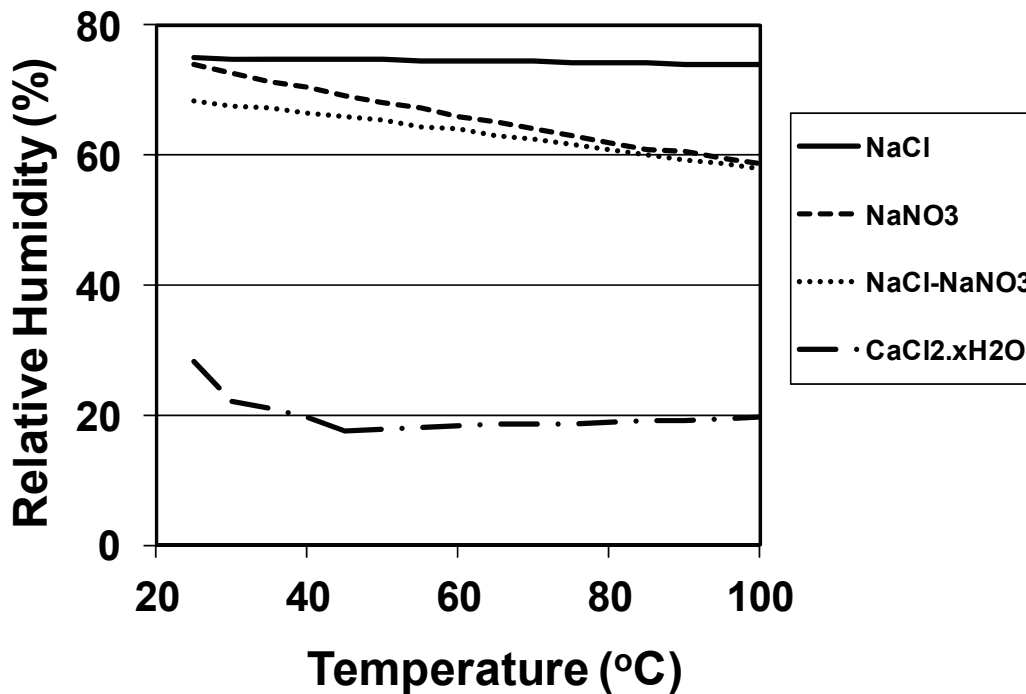


Figure 1: The Deliquescence Behaviour of Commonly Observed Salt Contaminants

The RH in the bentonite pores is determined by the suction behaviour of the buffer. Figure 2 shows the suction behaviour of MX80 bentonite as a function of buffer density (Man and Martino 2009). The suction potential (S_r) is a function of the degree of saturation (S) (Luckner et al. 1989)

$$S_r = \frac{[(S^{-1})^{1/m} - 1]^{1/n}}{\alpha} \quad (1)$$

where the fitting parameters m , n , and α are functions of the effective montmorillonite dry density (EMDD); for an EMDD = $1.432 \text{ Mg}\cdot\text{m}^{-3}$ for highly compacted bentonite, these parameters have values of 0.671, 1.36, and 0.0289 MPa^{-1} , respectively (Man and Martino 2009).

The suction potential is equal and opposite in sign to the water potential (Ψ) which, in turn, is related to the water activity (a_w) by (Brown 1990)

$$-S_r = \Psi = \frac{RT}{V_w} \ln a_w \quad (2)$$

where R is the gas constant, T is the absolute temperature, and V_w is the molar volume of water. The water activity is equal to the RH (expressed as a fraction). Combining Equations (1) and (2), therefore, gives an expression for the RH in terms of the degree of saturation, namely

$$\text{RH} = a_w = \exp\left(\frac{-V_w [(S^{-1})^{1/m} - 1]^{1/n}}{RT\alpha}\right) \quad (3)$$

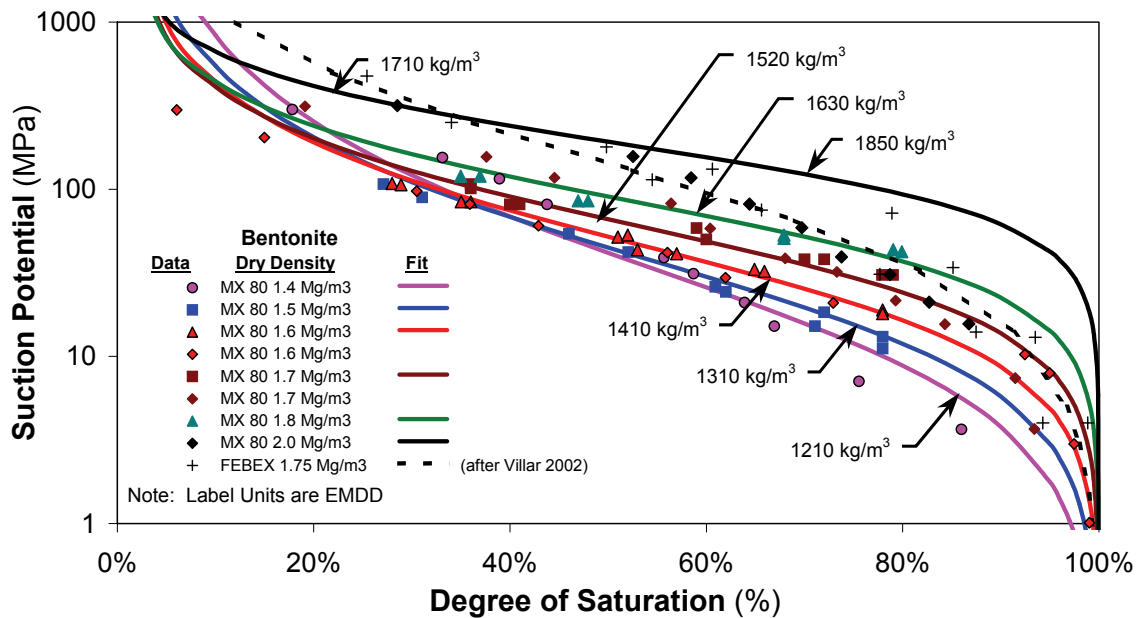


Figure 2: Suction Potential of MX80 Bentonite as a Function of the Degree of Saturation and Buffer Density (Man and Martino 2009)

Figure 3 shows the dependence of the suction potential and RH (or a_w) on the degree of saturation based on Equations (1) and (3), respectively. These expressions, along with a knowledge of the nature of the surface contaminants, can be used to assess at what stage the UFC surface will become wetted as the repository saturates.

A number of other environmental parameters, in addition to the temperature, RH, and redox conditions, also affect the general corrosion behaviour of the container, including:

Pore-water chemistry: Under saturated conditions, the container surface will be in contact with bentonite pore water. At least initially, the composition of the pore water may differ from that of the ground water. Eventually, however, the pore water will equilibrate with the ground water.

pH: Calcite minerals in the bentonite will effectively buffer the pH in the range pH 7-8.

Mass transport: The low hydraulic conductivity of compacted sodium bentonite will limit mass transport to diffusion only. During the aerobic phase, the rate of corrosion may be limited by the rate of transport of O_2 to the container surface, although the diffusivity of O_2 in unsaturated bentonite is high (King et al. 1996).

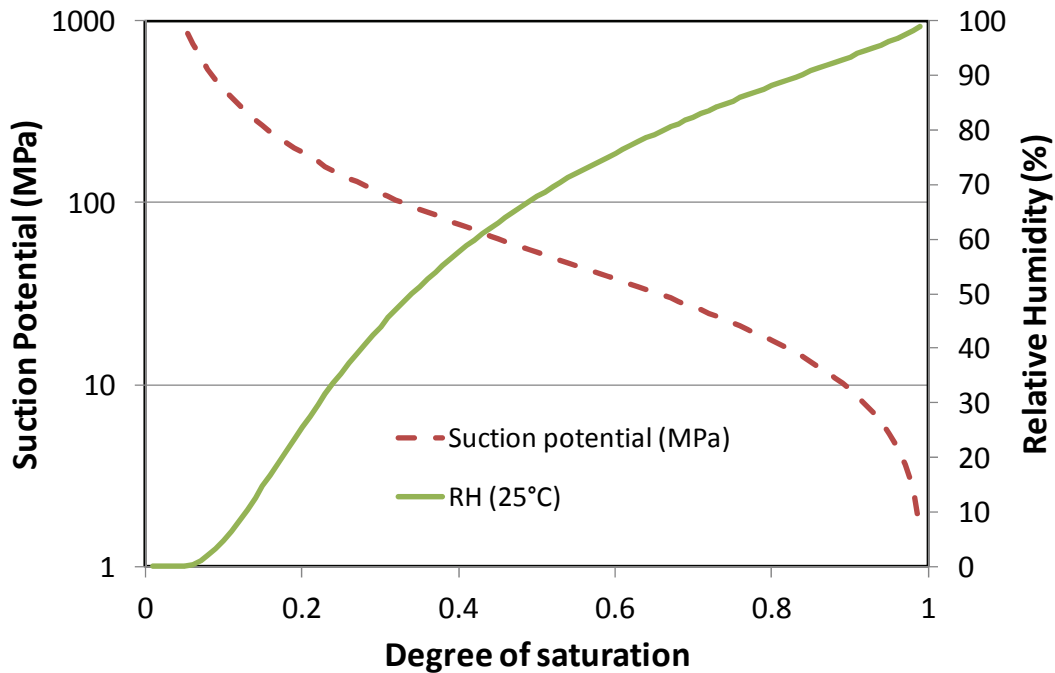


Figure 3: Dependence of the Suction Potential and Relative Humidity on the Degree of Saturation for Highly Compacted Bentonite Based on Equations (1) and (3), Respectively

Radiation:	Gamma radiolysis of water will produce oxidising and reducing radiolysis products. However, the maximum surface absorbed dose rate for a 10-cm-thick C-steel UFC will be $<1 \text{ Gy}\cdot\text{h}^{-1}$ and there will be no significant effect on the corrosion rate (Shoesmith and King 1999).
Operational phase:	It is implicitly assumed that there is no significant corrosion prior to the sealing of the repository. An extended operational phase could allow O_2 ingress and additional corrosion of the container.
Microbial activity:	Microbial activity is suppressed by the presence of highly compacted bentonite and saline solutions (Stroes-Gascoyne et al. 2006, 2007, 2008). Therefore, microbial activity is unlikely close to the container and there will be no effect on the general corrosion behaviour.
Stress:	Applied and residual stresses affect the environmentally assisted cracking behaviour of the container but have no effect on general corrosion.
Mineral impurities:	Mineral impurities in the host rock (e.g., pyrite) will have an insignificant effect on the general corrosion behaviour of the container.

3. REVIEW OF CORROSION INFORMATION

3.1 DRY AIR OXIDATION

Prior to the formation of liquid water on the container surface, corrosion will take the form of slow oxidation in "dry" air. (Dry air may contain some water vapour but insufficient to form a liquid phase). Oxidation of the UFC will result in the formation of a duplex $\text{Fe}_3\text{O}_4/\text{Fe}_2\text{O}_3$ surface film (Desgranges et al. 2003). Oxide growth can be modelled in terms of the reaction



Oxidation kinetics for Fe and a low-alloy steel have been found to follow both parabolic and logarithmic rate laws, although parabolic kinetics have generally been assumed for modelling purposes (Desgranges et al. 2003, Larose and Rapp 1997, Terlain et al. 2001). The weight gain W as a function of time t is given by

$$W^2 = K_p \cdot t \quad (5)$$

where K_p is the temperature-dependent parabolic rate constant given by

$$K_p = K_0 \exp\left(-\frac{E_a}{RT}\right) \quad (6)$$

where K_0 is a pre-exponential factor and E_a the activation energy.

Desgranges and co-workers (Desgranges et al. 2003, Terlain et al. 2001) studied the oxidation of both high-purity Fe and a low-alloy steel containing 0.40 wt.% C and 0.33 wt.% Cr. Data for Fe for temperatures between 100°C and 400°C gave a temperature-dependent parabolic rate constant of

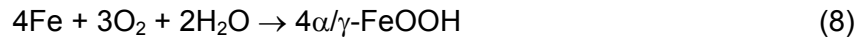
$$K_p = 2.648 \times 10^4 \exp\left(-\frac{97,500}{RT}\right) \text{ mg}^2 \cdot \text{cm}^{-4} \cdot \text{s}^{-1} \quad (7)$$

where the activation energy is 97.5 kJ/mol.

The Fe exhibited faster oxidation than the low alloy steel, which is somewhat unexpected as the rate generally increases with increasing C content (Larose and Rapp 1997). The oxidation rate was independent of the moisture content of the atmosphere (within the range studied of 2-12 vol.% H₂O) and the effect of O₂ partial pressure was not determined. Experiments were performed for a maximum period of 700 h (generally ≤600 h) and it is not clear whether there were periodic increases in the oxidation rate due to spalling of the thickening oxide.

3.2 AEROBIC UNSATURATED CONDITIONS

Once the container surface is wetted by liquid water, a period of aerobic corrosion under unsaturated conditions is expected to occur (assuming that all of the initially trapped O₂ has not been consumed by oxidation of the container). Corrosion will result in the consumption of O₂ and H₂O, but not the generation of H₂. The nature of the corrosion reaction depends, in part, on the presence of anions such Cl⁻, SO₄²⁻, and CO₃²⁻ which will lead to the formation of various forms of green rust. Since the nature of the surface deposits is not precisely known, the overall corrosion reaction will be described here by the formation of a hydrated Fe(III) species



with the α- and γ- forms representing goethite and lepidocrocite, respectively. Depending on the RH and the distribution of surface salt contaminants, the corrosion reaction may be more or less localised. Localised corrosion will be favoured by low RH and a sparse distribution of surface salts.

There have been a large number of studies of the corrosion behaviour of C-steel under aerobic conditions, with those specifically performed as part of nuclear waste management programmes having been summarised by King (2005) and King and Stroes-Gascoyne (2000). These studies have resulted in a wide range of reported corrosion rates (from <1 μm·a⁻¹ to >100 μm·a⁻¹), reflecting the wide range of experimental conditions used, including:

- exposure periods from 100 h to 5 a;
- environments including saturated buffer and backfill, bulk solution, and humid atmospheres;
- continuously aerated and initially aerated conditions;
- with and without radiation;
- fresh water to simulated salt brine inclusions;
- pH from near-neutral to >pH 10;
- temperatures from ambient to 170°C;
- various ferrous alloys including cast iron, ductile cast iron, various grades of carbon steel, pure Fe, normalised cast steel, forged steel, and Ferrovac E;
- planar, U-bend (stressed), and welded samples; and
- surface finishes ranging from as-received to highly polished.

Of these factors, the ones that have the greatest effect are the exposure time, the nature of the environment, and temperature. Figure 4 shows a compilation of selected data and illustrates the effect of temperature on the aerobic corrosion rate in saturated backfill,¹ bulk solution,² and in humid atmospheres.³ In selecting these data, only rates for exposure periods greater than 2000 h have been shown, since this is the minimum period for the establishment of a steady-state corrosion rate (King 2008, Newman et al. 2010). All of the rates in Figure 4 were determined in the absence of radiation, since the only data available for irradiated systems are from studies with extremely high radiation fields (of the order of 100-10,000 Gy·h⁻¹).

There is no clear trend of the corrosion rate with temperature in Figure 4. The rates in (granite or clay) backfill tend to be lower than those in bulk solution or under atmospheric conditions presumably because the rate is limited by the diffusion of O₂ through the saturated backfill (Honda et al. 1991, King 2007). The limited number of data from atmospheric corrosion studies (approximate RH of 75%, Casteels et al. 1986, Debruyne 1990) tend to give higher corrosion rates than in bulk solution, possibly because of faster O₂ supply or because of the presence of SO₂ added to simulate oxidation products of Belgian Boom Clay.

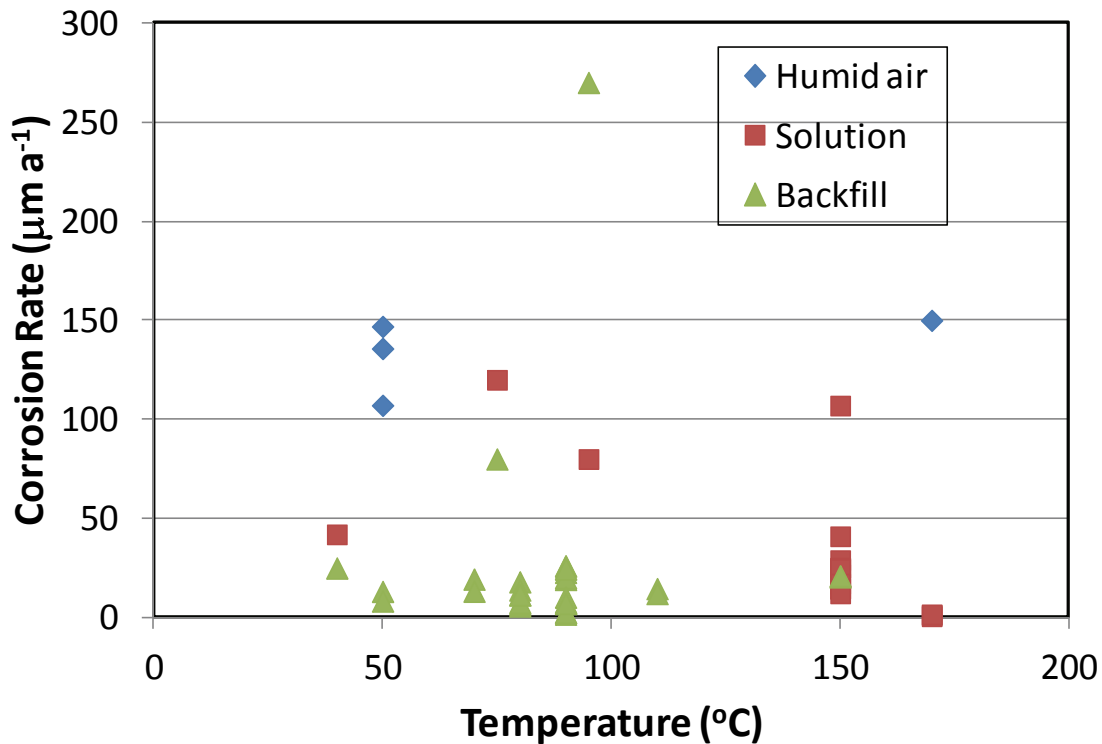


Figure 4: The Effect of Temperature on the Aerobic Corrosion Rate of Steel in Humid Air, Bulk Solution, and in the Presence of Backfill Material

¹ The nature of the backfill varied between the different studies and consisted of either crushed granite, compacted Kunigel bentonite, or Boom Clay. All were saturated with the respective aerated synthetic ground water solutions.

² Data are presented for various aerated solutions, ranging from distilled water, through simulated interstitial clay water with a salinity of the order of 100 mg/L, to simulated intrusion brines with a salinity of 100,000's mg/L.

³ Relative humidity approximately 75%.

Figure 5 shows the same data from Figure 4 plotted in Arrhenius format, along with the proposed expression of Foct and Gras (2003) for the aerobic corrosion rate. The latter was based on a review of aerobic corrosion rates, with an emphasis on data from studies with backfill and is given by

$$\text{Rate} = 1042 \exp\left(-\frac{1340}{T}\right) \mu\text{m} \cdot \text{a}^{-1} \quad (9)$$

where the corresponding activation energy of 11.4 kJ/mol is characteristic of rate control by diffusion through solution-filled pores.

The data in Figure 4 of most relevance to Phase 2 are those measured in humid air. Somewhat surprisingly, these rates show little effect of temperature. For comparison, the rates of atmospheric corrosion of C-steel measured under ambient conditions in different environmental settings are (Leygraf and Graedel 2000):

- rural: 4-65 $\mu\text{m} \cdot \text{a}^{-1}$
- urban: 23-71 $\mu\text{m} \cdot \text{a}^{-1}$
- industrial: 26-175 $\mu\text{m} \cdot \text{a}^{-1}$
- marine: 26-104 $\mu\text{m} \cdot \text{a}^{-1}$

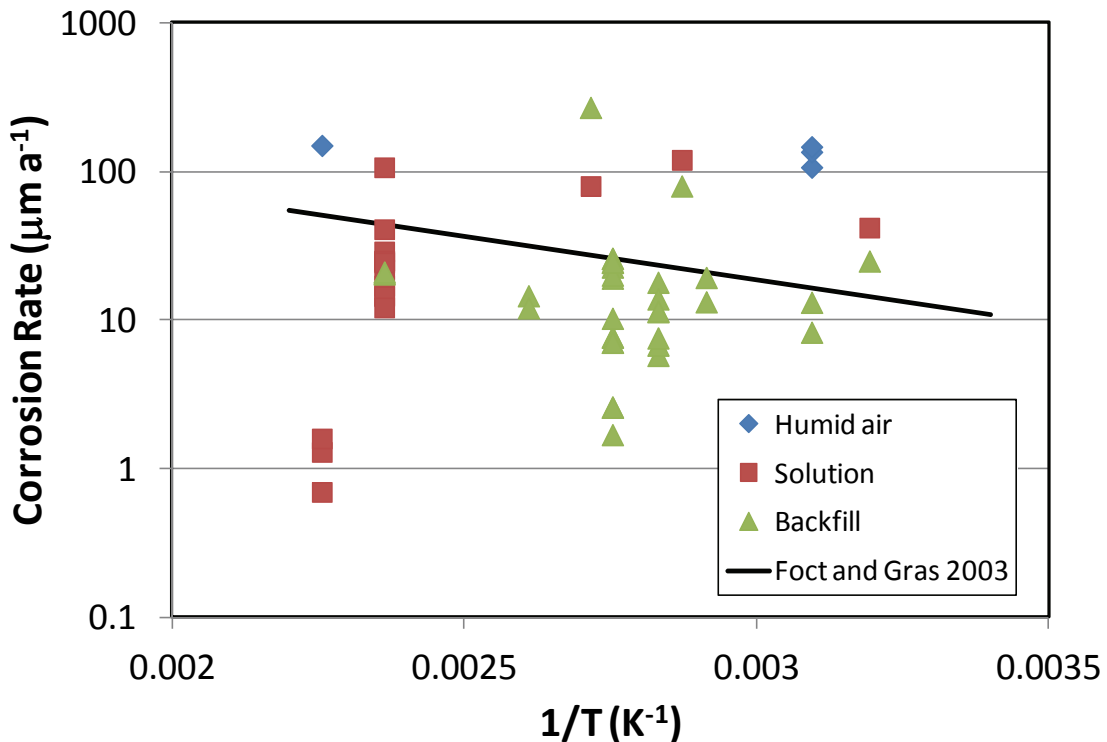


Figure 5: Arrhenius Plot of the Aerobic Corrosion Rate Data from Figure 4

There are no studies in which the aerobic corrosion rate of steel has been determined as a function of RH.

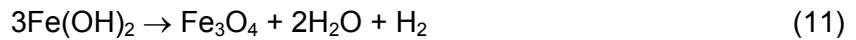
The threshold RH for atmospheric corrosion is independent of the redox conditions and will be the same for Phases 2 and 3 (see the discussion in Section 3.3).

3.3 ANAEROBIC UNSATURATED CONDITIONS

In the absence of O₂, C-steel corrodes with the evolution of H₂



Ferrous hydroxide can convert to magnetite via the Schikkor reaction



The overall stoichiometry for the formation of Fe₃O₄, therefore, and the most conservative from the viewpoint of H₂ production, is



There are few studies of the anaerobic atmospheric corrosion of C-steel in the literature, primarily because it is not, with the present exception, an environment of significant industrial interest. Newman et al. (2010) have reported the results of a detailed study of the anaerobic corrosion of C-steel as a function of RH and temperature over periods up to 3355 h (140 d). Specimens were used in the as-cleaned, pickled, and pre-corroded conditions, the latter following pre-exposure to 0.05 mol·dm⁻³ or 0.5 mol·dm⁻³ NaCl solution. Corrosion rates were determined based on the rate of H₂ evolution. The rates reported for the as-cleaned and pickled samples were extremely low (<0.01 μm·a⁻¹) but, as these surface conditions are not considered relevant to a UFC in a repository, are not considered further here.

In all cases, the corrosion rate was found to decrease with time, primarily due to the formation of a protective surface film. A steady-state corrosion rate was observed in some experiments after an exposure time of 1500-2000 h (Figure 6). In most cases, however, the rate continued to decrease with time for the entire duration of the test (up to 2500-3000 h).

In general, the corrosion rate increased with increasing temperature. Figure 7 shows an Arrhenius plot of the steady-state rates from Figure 6, the apparent steady-state rate at a temperature of 70°C from the same study (albeit determined from an experiment with a relatively short exposure period of only 213 hrs), and a rate at 170°C in a 100% humid clay atmosphere from Debruyne (1990). The rates from the two studies appear to show a consistent temperature dependence with an activation energy of 44.3 kJ/mol. The corrosion rate expression for C-steel under anaerobic conditions at 100% RH based on these data is given by

$$\text{Rate} = 8.89 \times 10^6 \exp\left(-\frac{5332}{T}\right) \mu\text{m} \cdot \text{a}^{-1} \quad (13)$$

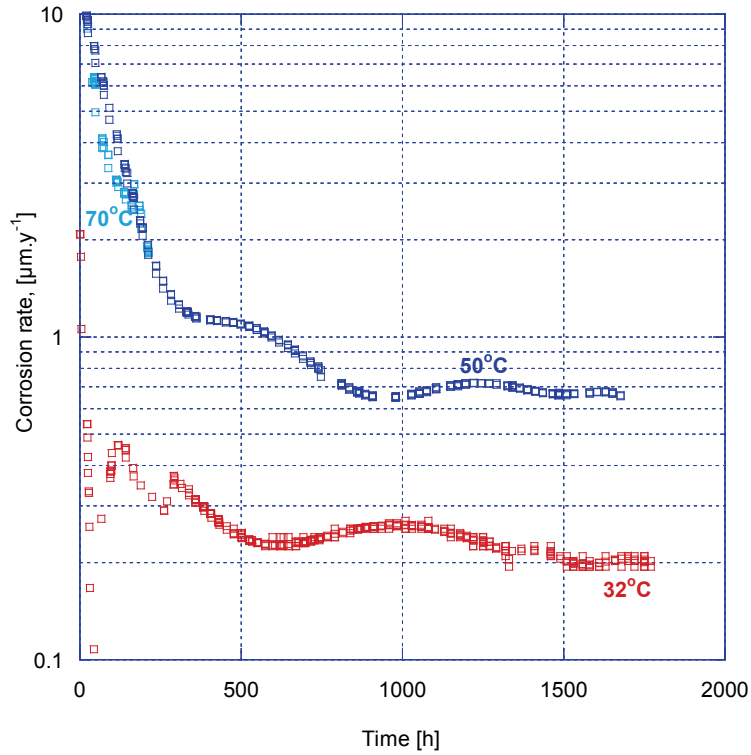


Figure 6: Effect of Temperature on the Time Dependence of the Corrosion Rate of Carbon Steel Under Anaerobic Conditions at 100% Relative Humidity Following Pre-corrosion in $0.5 \text{ mol}\cdot\text{dm}^{-3}$ NaCl Solution (Newman et al. 2010)

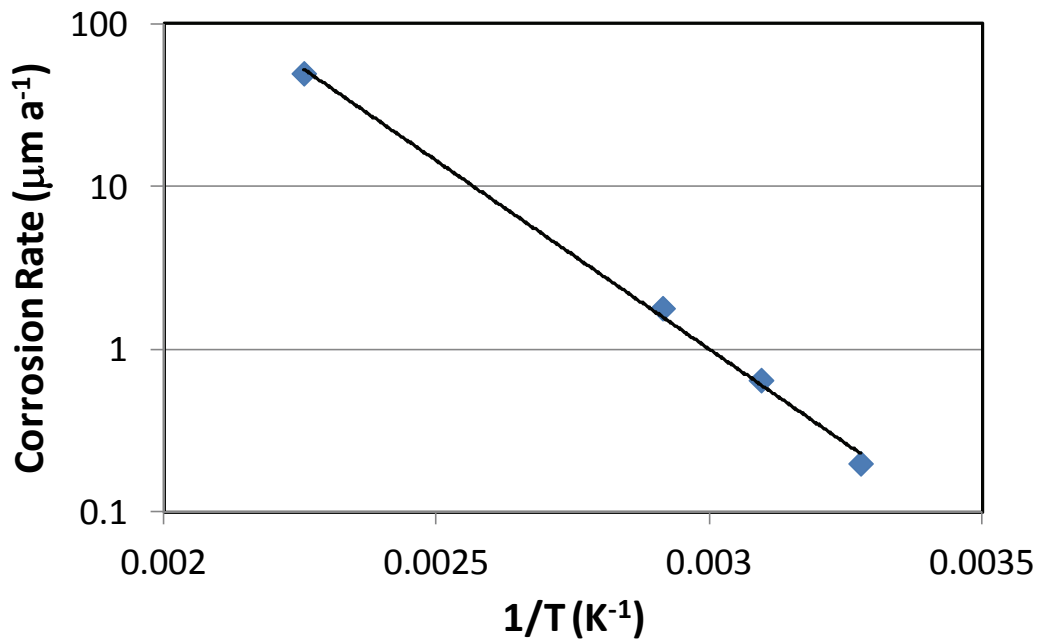


Figure 7: Arrhenius Plot of the Anaerobic Corrosion Rate of Carbon Steel at 100% Relative Humidity

The apparent consistency between the two sets of data may be partly fortuitous, as the experiments were performed under different conditions. For example, there is no indication that Debruyn (1990) pre-corroded his samples prior to exposure as did Newman et al. (2010). In addition, the fit is dependent on the results from single experiments, with no indication of the scatter in the data. Nevertheless, the magnitude of the derived activation energy is consistent with that expected for an activated process.

In addition to the rate of anaerobic corrosion under unsaturated conditions, the Newman et al. (2010) study also provides useful evidence for the threshold RH and the effect of RH on the corrosion rate. Figure 8 shows the time dependence of the corrosion rate of pre-corroded C-steel at 32°C as a function of the RH (controlled by equilibrating the atmosphere with various solutions of known water activity). The DRH for NaCl at 32°C is $75.1 \pm 0.1\%$ (Rozenfeld 1972). Corrosion occurs at a RH as low as 68%, but this is likely because pre-corrosion has created a porous surface film that promotes water condensation by capillary action as well as by deliquescence. Thus, the threshold RH for the pre-corroded surface is $\leq 68\%$, but there is no systematic effect of RH on the corrosion rate above this threshold.

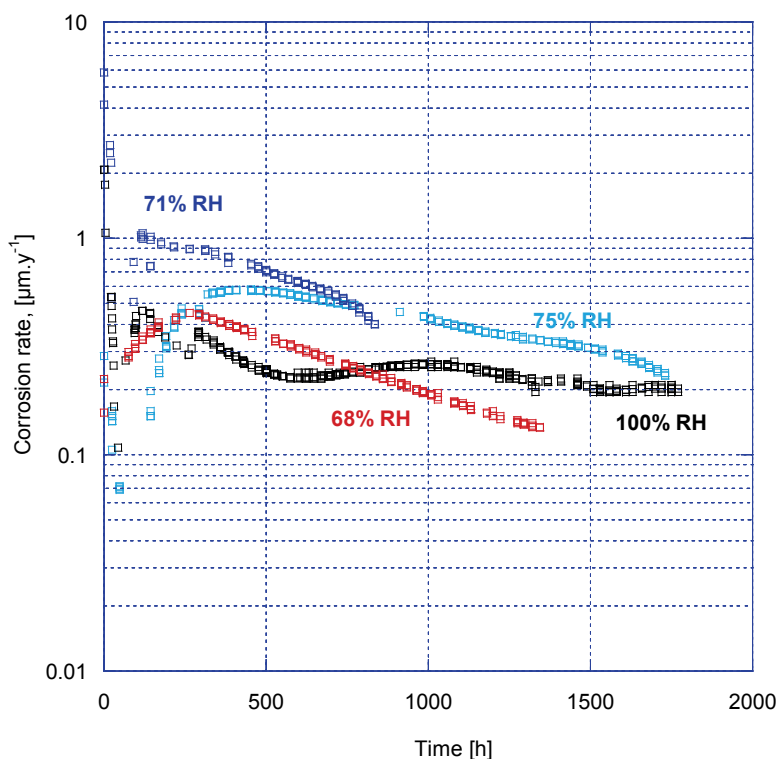


Figure 8: Effect of Relative Humidity on the Time Dependence of the Corrosion Rate of Carbon Steel Under Anaerobic Conditions at 32°C Following Pre-corrosion in $0.5 \text{ mol}\cdot\text{dm}^{-3}$ NaCl Solution (Newman et al. 2010)

Figure 9 shows similar data measured at a temperature of 50°C, but at RH values above (75% and 100%) and below (51% and 30.5%) the DRH for NaCl (74.1% at 50°C, Rozenfeld 1972). It is interesting to note that whilst apparently sustained corrosion occurs at RH values above the DRH, the rate of corrosion decreases with time for RH below the threshold and effectively stops after 500-1000 h (i.e., the corrosion rate drops to $\leq 1 \text{ nm}\cdot\text{a}^{-1}$). These results suggest that the threshold RH for unsaturated corrosion is of the order of 70% RH, consistent with the thermodynamically predicted value based on surface contamination by NaCl. The fact that corrosion occurs at all at RH levels below the DRH suggests that pre-corrosion created porous corrosion products that condense water by capillary action at levels below the thermodynamically predicted threshold RH. However, the fact that this corrosion is not apparently sustained indicates that this is a transitory effect.

The other important observation of Newman et al. (2010) is the nature of the film formed as a result of anaerobic corrosion. Detailed surface analysis indicates the formation of Fe_3O_4 as the predominant corrosion product, suggesting that corrosion under unsaturated anaerobic conditions can be represented by Reaction (12).

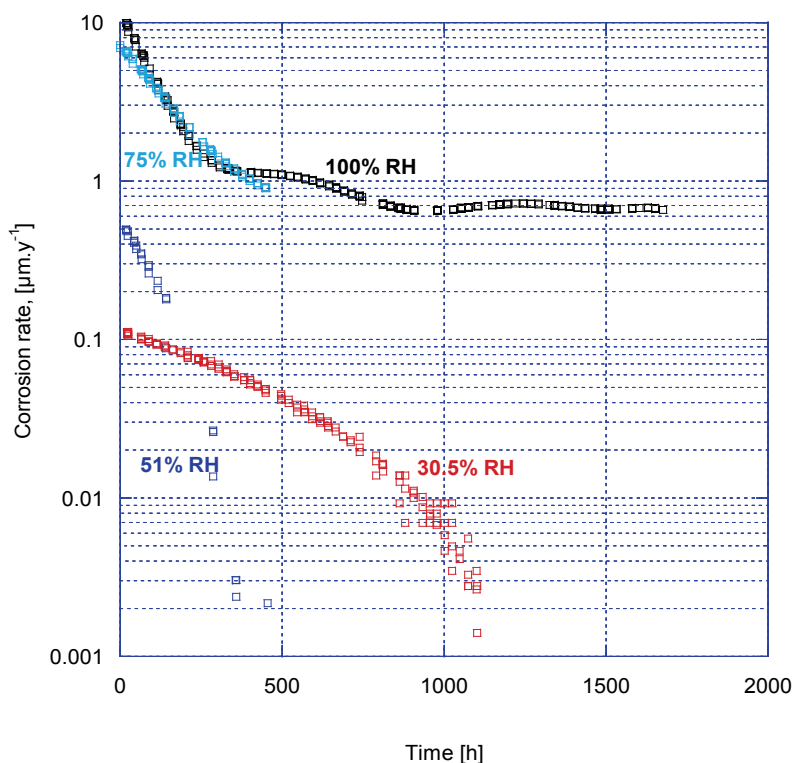


Figure 9: Effect of Relative Humidity on the Time Dependence of the Corrosion Rate of Carbon Steel Under Anaerobic Conditions at 50°C Following Pre-corrosion in $0.5 \text{ mol}\cdot\text{dm}^{-3}$ NaCl Solution (Newman et al. 2010)

3.4 ANAEROBIC SATURATED CONDITIONS

At some stage following the onset of anaerobic conditions, the buffer and backfill materials will become saturated with ground water. The corrosion behaviour of C-steel in saturated compacted bentonite under anaerobic conditions has been studied in a number of national nuclear waste management programs (King 2008). There are differences between the corrosion behaviour of steel in bulk solution and in compacted bentonite (Figure 10; Johnson and King 2008, King 2008). The corrosion rate tends to be higher in the presence of clay because of the formation of a less-protective carbonate-based film rather than the Fe_3O_4 film formed in bulk solution. Furthermore, the corrosion rate reaches an apparent steady state faster in bulk solution than in compacted clay.

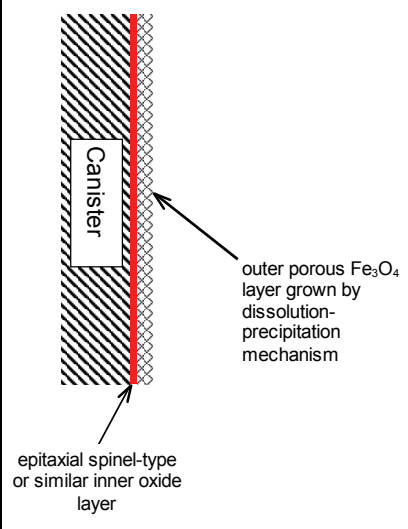
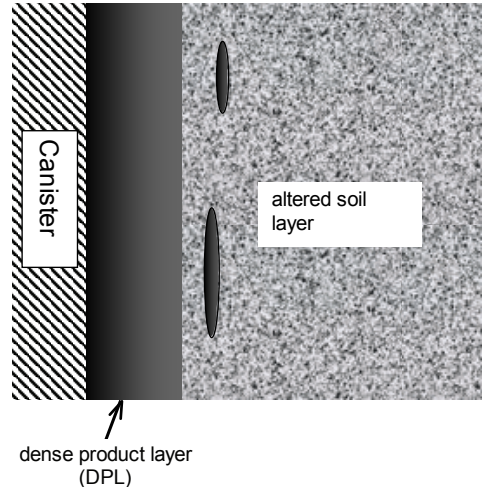
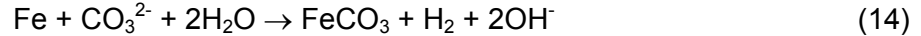
	Bulk solution	Compacted clay
Corrosion rate and time dependence	~0.1 $\mu\text{m a}^{-1}$ Steady-state after 4-6 months	~1 $\mu\text{m a}^{-1}$ Still decreasing after 4 a
Corrosion products: composition and structure	Duplex spinel-type/ Fe_3O_4 structure 	Corrosion product layer containing $FeCO_3/(Fe,Ca)CO_3$ and adjoining altered soil layer 

Figure 10: Summary of Differences Between the Anaerobic Corrosion Behaviour of Carbon Steel in Bulk Solution and in Compacted Clay (Johnson and King 2008, King 2008)

In the presence of compacted bentonite, C-steel corrodes with the formation of a carbonate-containing corrosion product (Papillon et al. 2003; King 2007, 2008). The source of carbonate is calcite and other carbonate minerals in the bentonite (or in the host rock). The overall stoichiometry of the corrosion reaction can be written as:



Iron carbonate, or some form of FeCO_3 incorporating cations from the pore solution, will predominate until such time that all carbonate minerals in the clay have been consumed (Wersin et al. 2007). As and when this occurs, the predominant corrosion reaction is then likely to be the formation of Fe_3O_4 according to Reaction (12). This transition in corrosion reactions will have a small impact on the extent of H_2 formation as the formation of FeCO_3 results in the formation of 1 mol H_2 per mol of Fe, whereas the formation of Fe_3O_4 results in the formation of 1.33 mol H_2 per mol of Fe. However, because of the difference in protectiveness of FeCO_3 and Fe_3O_4 (the magnetite being significantly more protective), the rate of H_2 generation is likely to be lower once the corrosion reaction changes to the formation of Fe_3O_4 instead of FeCO_3 .

Figure 11 shows a compilation of corrosion rates from tests in compacted bentonite as a function of temperature. There is significant scatter in the data, partly the result of different exposure periods in the different tests. Tests with exposure periods greater than 12 months (indicated by the open symbols in Figure 11) tend to give lower corrosion rates than shorter tests.

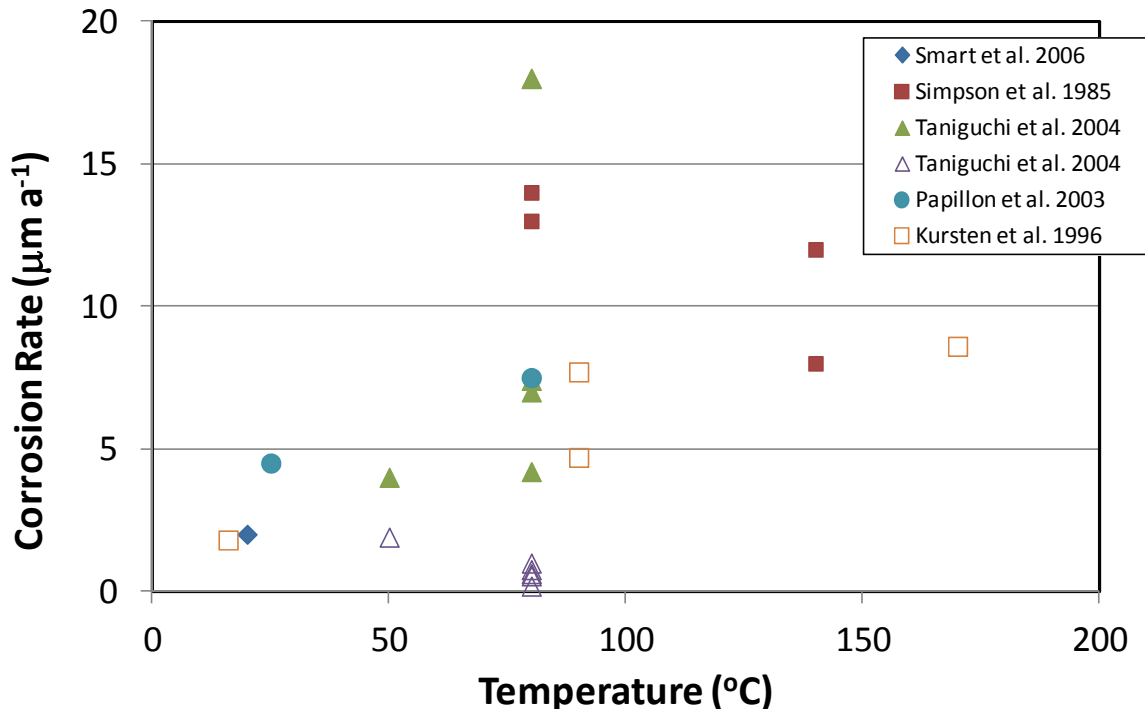


Figure 11: Temperature Dependence of the Corrosion Rate of Carbon Steel in Compacted Clay. Tests with exposure periods of 12 months or less are shown as filled symbols, with results from longer tests shown as open symbols

In general, however, the corrosion rate increases with increasing temperature. Figure 12 shows the data from Figure 11 in Arrhenius format, along with an expression for the temperature dependence proposed by Gras (1996), given by

$$\text{Rate} = 8200 \exp\left(-\frac{2435}{T}\right) \mu\text{m} \cdot \text{a}^{-1} \quad (15)$$

corresponding to an activation energy of 20.2 kJ/mol. The Gras (1996) expression appears to conservatively estimate the long-term anaerobic corrosion rate of C-steel in compacted clay.

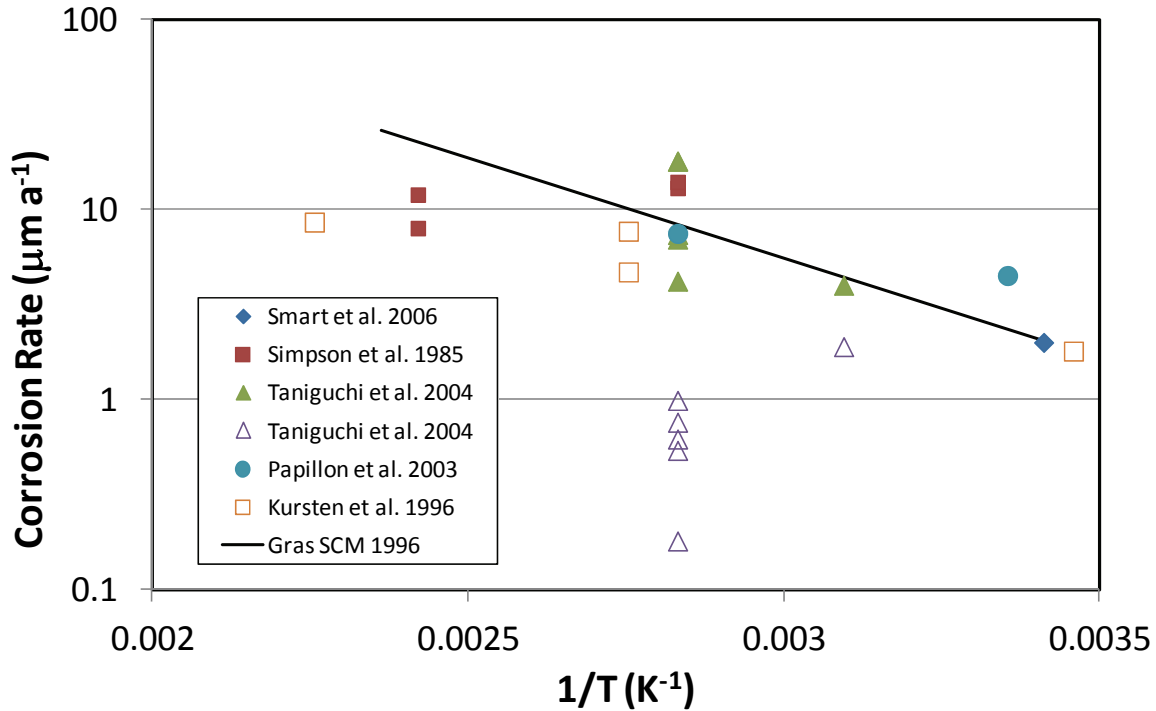


Figure 12: Arrhenius Plot of the Temperature Dependence of the Corrosion Rate of Carbon Steel in Compacted Clay Based on the Data in Figure 11. Also shown on the figure is a proposed dependence by Gras (1996)

3.5 TRANSITION BETWEEN PHASES

The different phases in the evolution of the environment result in different rates of corrosion and different types of corrosion product. For example, experimental studies for the individual phases indicate the following corrosion products:

- Phase 1: Fe_2O_3
- Phase 2: $\alpha/\gamma\text{-FeOOH}$ (and other forms of hydrated Fe(III) solids)
- Phase 3: Fe_3O_4
- Phase 4: $(\text{Fe,Ca})\text{CO}_3$ (Fe_3O_4 in absence of carbonate)

Thus, there will likely be a transformation of corrosion products as the environmental conditions evolve, but which is not explicitly considered here. Furthermore, the reductive dissolution of

Fe(III) solids formed during Phases 1 and 2 could support additional Fe dissolution which, again, is not explicitly considered here.

4. RECOMMENDED CORROSION RATE DATA

4.1 PHASE 1 DRY AIR OXIDATION

The studies of Desgranges and co-workers (Desgranges et al. 2003, Terlain et al. 2001) represent a reliable database for the oxidation of Fe and steel in air at the relatively low temperatures (100°C to 400°C) of interest here.

The following assumptions have been made in deriving the best-estimate oxidation rate expression given below:

- Oxidation is assumed to follow parabolic kinetics, as found experimentally by Desgranges et al. (2003) and as widely reported by Larose and Rapp (1997).
- The kinetic data for Fe are used in preference to those for the low alloy steel studied by Desgranges et al. (2003), the Fe data being more conservative.
- The observed mass gain is assumed to result from the oxidation of Fe to Fe₂O₃.
- The parabolic kinetic rate constant given by Equation (7) is assumed to describe the kinetics of the oxidation of a C-steel UFC.
- The rate of oxidation is assumed to be independent of the O₂ partial pressure (except that the rate is zero in the absence of O₂).

Expressed in terms of a penetration rate, the best estimate rate of oxidation of C-steel during Phase 1 (R₁) is given by

$$R_1 = \frac{A_1 \exp\left(\frac{-5864}{T}\right)}{t^{1/2}} \quad \mu\text{m}\cdot\text{a}^{-1} \quad (16)$$

where t is the time in years from the time of emplacement and the pre-exponential term A₁ is assigned a best-estimate value, as well as lower and upper bounds.

The best estimate value for A₁ is taken to be 1.353 x 10⁻⁶ μm·a⁻¹ based on the data of Desgranges et al. (2003). In deriving the expression for R₁, it is assumed that the mass change for Reaction (4) corresponds to 24 g·mol_{Fe}⁻¹, and that the molar mass and density of Fe (or C-steel) are 55.85 g·mol⁻¹ and 7.86 g·cm⁻³, respectively. Although there are relatively few data available, it is not unreasonable to expect that the lower and upper bound corrosion rates might differ by a factor of ten. In the absence of other information, it is assumed here that the best-estimate value is the (geometric) mean of the lower and upper bound values. Thus, the values of A₁ for the lower and upper bound estimates are 4.279 x 10⁵ μm·a⁻¹ and 4.279 x 10⁶ μm·a⁻¹, respectively.

The overall stoichiometry of the corrosion reaction is given by:



As an indication of the slow rate of air oxidation, Equation (16) predicts a depth of corrosion of only 13 μm in 1000 a at a constant temperature of 100°C.

The time dependence of the corrosion rate is explicitly included in Equation (16).

Within the range of experimental conditions studied (2-12 vol.% H₂O), there is no effect of RH on the oxidation rate (Desgranges et al. 2003, Terlain et al. 2001).

In the absence of evidence to the contrary, the oxidation rate is assumed to be independent of the O₂ partial pressure.

4.2 PHASE 2 AEROBIC UNSATURATED CONDITIONS

The overall stoichiometry of the corrosion reaction during Phase 2 is assumed to be given by:



As discussed in Section 3.2, there is a large number of studies of the aerobic corrosion of C-steel (with a correspondingly large scatter in the reported rates), although there have been relatively few studies in humid atmospheres. Figure 13 shows the data from Figure 5 measured in bulk solution and humid air, along with the proposed best-estimate and lower and upper bound fits to the data. In each case, the slope of the fit corresponds to the activation energy proposed by Foct and Gras (2003). The expression for the proposed corrosion rate is

$$R_2 = A_2 \exp\left(-\frac{1340}{T}\right) \mu\text{m} \cdot \text{a}^{-1} \quad (19)$$

where A_2 is the pre-exponential term for Phase 2 which has a best-estimate value of $4168 \mu\text{m} \cdot \text{a}^{-1}$ and values of $1042 \mu\text{m} \cdot \text{a}^{-1}$ and $10420 \mu\text{m} \cdot \text{a}^{-1}$ for the lower- and upper-bound fits, respectively. The best-estimate value was selected to provide a reasonable fit to the experimental data from humid-air tests and a number of the tests from bulk solution. The lower-bound value of A_2 corresponds with the original expression of Foct and Gras (2003) and the upper-bound value gives corrosion rates ten times greater than those of Foct and Gras (2003) and encompasses all of the measured values.

It should be noted that the corrosion rate under unsaturated aerobic conditions is, in general, so high that the duration of Phase 2 will be short (< 1 a) because of the limited amount of O₂ in the repository.

Although the time dependence of the corrosion rate may be significant over the short duration of the aerobic unsaturated phase, no time dependence is included because of the lack of suitable data and the relative lack of importance of this period in the current assessment.

In the absence of evidence to the contrary, the corrosion rate is assumed to be independent of the O₂ partial pressure.

The transition from Phase 1 to Phase 2 is assumed to occur at a threshold RH at which the UFC surface becomes wetted by liquid water. The threshold RH depends on the nature of the surface and, in particular, the nature of surface salt contaminants, but is independent of the redox conditions (except inasmuch as aerobic corrosion may produce corrosion product morphology that differs from that under anaerobic conditions).

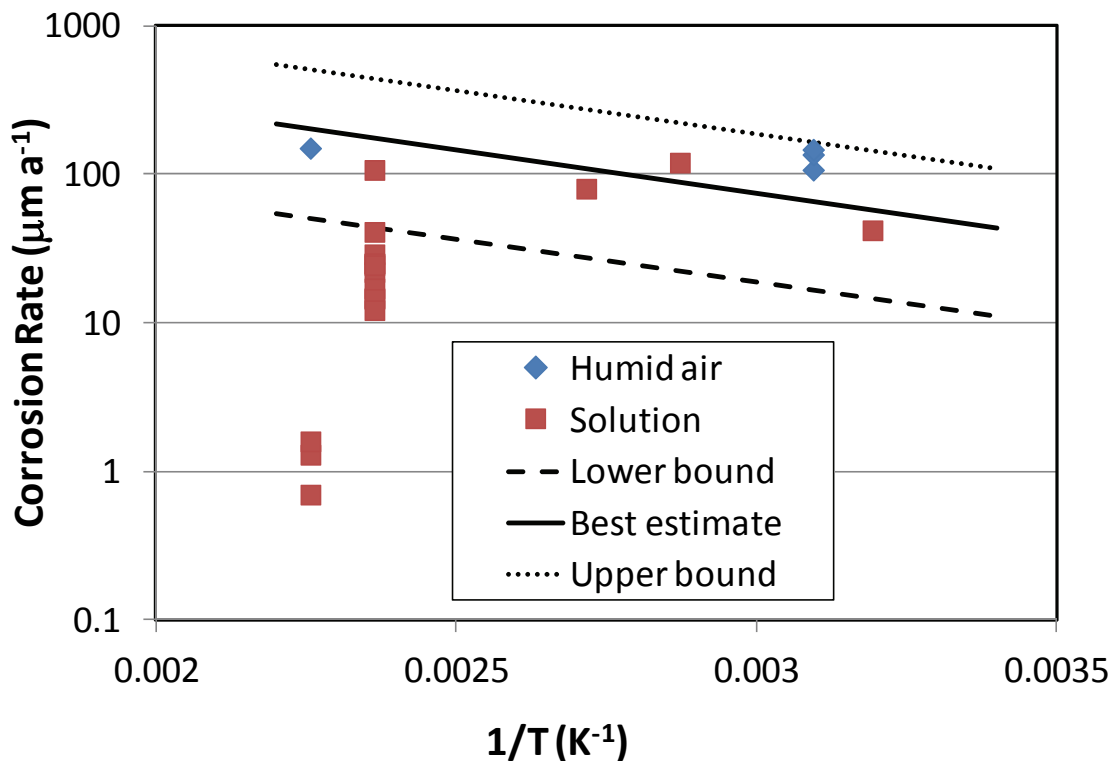


Figure 13: Proposed Corrosion Rate Expressions for the Aerobic Unsaturated Period Compared with Measured Corrosion Rates in Aerated Solution and Humid Air

In the absence of more-definitive information, let us assume that the surface wetting of the UFC is primarily determined by the deliquescence behaviour of NaCl. The evidence presented by Newman et al. (2010) under anaerobic conditions (and which we are assuming here applies equally to aerobic conditions) suggests a threshold RH slightly lower than the thermodynamic DRH of 70-75% and relatively little dependence of the corrosion rate on the RH at values higher than the threshold.

For the current modelling purposes, therefore, we will define a narrow range of RH over which the corrosion rate increases linearly from zero to the rate observed at 100% RH for the best-estimate case. This range of RH is defined by a lower threshold (critical) RH ($RH_{CRIT,L}$) and an upper threshold RH ($RH_{CRIT,U}$). The use of a range for the threshold RH is also of benefit computationally since it avoids step changes in the corrosion rates in the model.

Based on the results of Newman et al. (2010) and on evidence from the atmospheric corrosion literature (Leygraf and Graedel 2000, Rozenfeld 1972), the lower and upper threshold RH (expressed as a fraction) are given by:

$$RH_{CRIT,L} = 0.60 \quad (20a)$$

and

$$RH_{CRIT,U} = 0.80 \quad (20b)$$

To account for variability in the nature of the surface salt contaminants, upper and lower bound values are also defined for $RH_{CRIT,L}$ and $RH_{CRIT,U}$. Because of the presence of both Ca^{2+} and

Na⁺ ions in the ground and pore water, the lower bound values are defined on the basis that a mixed-salt deposit containing both CaCl₂·xH₂O and NaCl could form on the container surface. In this case, the lower-bound values are given by

$$RH_{\text{CRIT,L}} = 0.10 \quad (20c)$$

and

$$RH_{\text{CRIT,U}} = 0.20 \quad (20d)$$

In this case, wetting of the surface would occur at very low degrees of saturation and the lower-bound values can be considered conservative (in terms of the time at which aqueous corrosion begins). The upper bound critical RH values are based on the assumption that a salt less-deliquescent than NaCl is present on the container surface and are given by

$$RH_{\text{CRIT,L}} = 0.80 \quad (20e)$$

and

$$RH_{\text{CRIT,U}} = 0.90 \quad (20f)$$

Thus, the corrosion rate during Phase 2 is given by:

$$\text{for } RH \leq RH_{\text{CRIT,L}} \quad \text{Rate} = 0 \quad (21a)$$

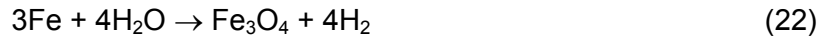
$$\text{for } RH_{\text{CRIT,L}} < RH \leq RH_{\text{CRIT,U}} \quad \text{Rate} = R_2 \left(\frac{RH - RH_{\text{CRIT,L}}}{RH_{\text{CRIT,U}} - RH_{\text{CRIT,L}}} \right) \quad (21b)$$

and

$$\text{for } RH > RH_{\text{CRIT,U}} \quad \text{Rate} = R_2 \quad (21c)$$

4.3 PHASE 3 ANAEROBIC UNSATURATED CONDITIONS

The overall stoichiometry of the corrosion reaction is given by:



Based on the data plotted in Figure 7 and the associated discussion, the expression for the best estimate of the temperature dependence of the anaerobic corrosion rate under unsaturated conditions at 100% RH is given by:

$$R_3 = A_3 \exp\left(-\frac{5332}{T}\right) \mu\text{m} \cdot \text{a}^{-1} \quad (23)$$

where the temperature dependence is given by the slope of Figure 7 and the pre-exponential term A_3 is assigned a best-estimate value, as well as lower and upper bounds.

The best-estimate value for the pre-exponential term A_3 is taken from the data in Figure 7 and is equal to $8.89 \times 10^6 \mu\text{m} \cdot \text{a}^{-1}$. Although there are relatively few data available, based on the observations under both aerobic unsaturated (Section 4.2) and anaerobic saturated (Section 4.4) conditions, it is not unreasonable to expect that the lower and upper bound corrosion rates under anaerobic unsaturated conditions might differ by a factor of ten. In the absence of other information, it is assumed here that the best-estimate value is the (geometric)

mean of the lower and upper bound values. Thus, the values of A_3 for the lower and upper bound estimates are $2.81 \times 10^6 \mu\text{m}\cdot\text{a}^{-1}$ and $2.81 \times 10^7 \mu\text{m}\cdot\text{a}^{-1}$, respectively. The dependence of the rate on RH is the same as that for aerobic unsaturated corrosion, namely:

$$\text{for } RH \leq RH_{\text{CRIT,L}} \quad \text{Rate} = 0 \quad (24a)$$

$$\text{for } RH_{\text{CRIT,L}} < RH \leq RH_{\text{CRIT,U}} \quad \text{Rate} = R_3 \left(\frac{RH - RH_{\text{CRIT,L}}}{RH_{\text{CRIT,U}} - RH_{\text{CRIT,L}}} \right) \quad (24b)$$

and

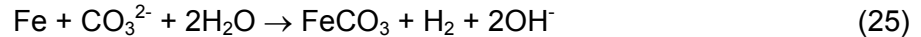
$$\text{for } RH > RH_{\text{CRIT,U}} \quad \text{Rate} = R_3 \quad (24c)$$

where the values of best-estimate and upper- and lower-bound values for $RH_{\text{CRIT,L}}$ and $RH_{\text{CRIT,U}}$ are defined by Equation (20). Equations (24a) and (24b) are only needed in the case where all of the initially trapped O_2 is consumed by oxidation of the container during Phase 1 (i.e., the duration of Phase 2 is zero). It is likely, however, that the RH will be greater than $RH_{\text{CRIT,U}}$ prior to the start of Phase 3 and that the rate during Phase 3 will be given by Equation (24c) at all times.

Based on the results of Newman et al. (2010), steady state is achieved after approximately 2000 h exposure. This period is considered to be short in comparison with the analysis period, so that the time dependence of the corrosion rate is not explicitly included here.

4.4 PHASE 4 ANAEROBIC SATURATED CONDITIONS

The overall stoichiometry of the corrosion reaction is given by:



Anaerobic corrosion to produce Fe_3O_4 (Reaction (22)) is also possible in saturated bentonite, especially if the carbonate content of the buffer pore solution is low or has been exhausted by the formation of FeCO_3 . Based on the data shown in Figure 12, the corrosion rate for Phase 4 is given by

$$R_4 = A_4 \exp\left(-\frac{2435}{T}\right) \mu\text{m}\cdot\text{a}^{-1} \quad (26)$$

where the temperature dependence corresponds to that proposed by Gras (1996) and the value of the pre-exponential factor for Phase 4 (A_4) is different for the best-estimate and upper and lower bound fits to the data.

The proposed fits to the experimental data are shown in Figure 14. The best-estimate fit corresponds to that proposed by Gras (1996), for which the pre-exponential factor has a value of $A_4 = 8200 \mu\text{m}\cdot\text{a}^{-1}$. The upper bound fit ($A_4 = 16400 \mu\text{m}\cdot\text{a}^{-1}$) was selected to bound all of the reported experimental data. The lower bound fit ($A_4 = 2050 \mu\text{m}\cdot\text{a}^{-1}$) was similarly selected to bound the majority of the reported data.

Experimental evidence suggests that the steady-state corrosion rate is only achieved after several years exposure to saturated compacted clay. However, this time dependence is not explicitly included here since it is considered to be short in comparison to the analysis period.

The transition from Phase 3 to Phase 4 is deemed to occur when the bentonite in contact with the UFC becomes completely saturated, subject to the availability of carbonate.

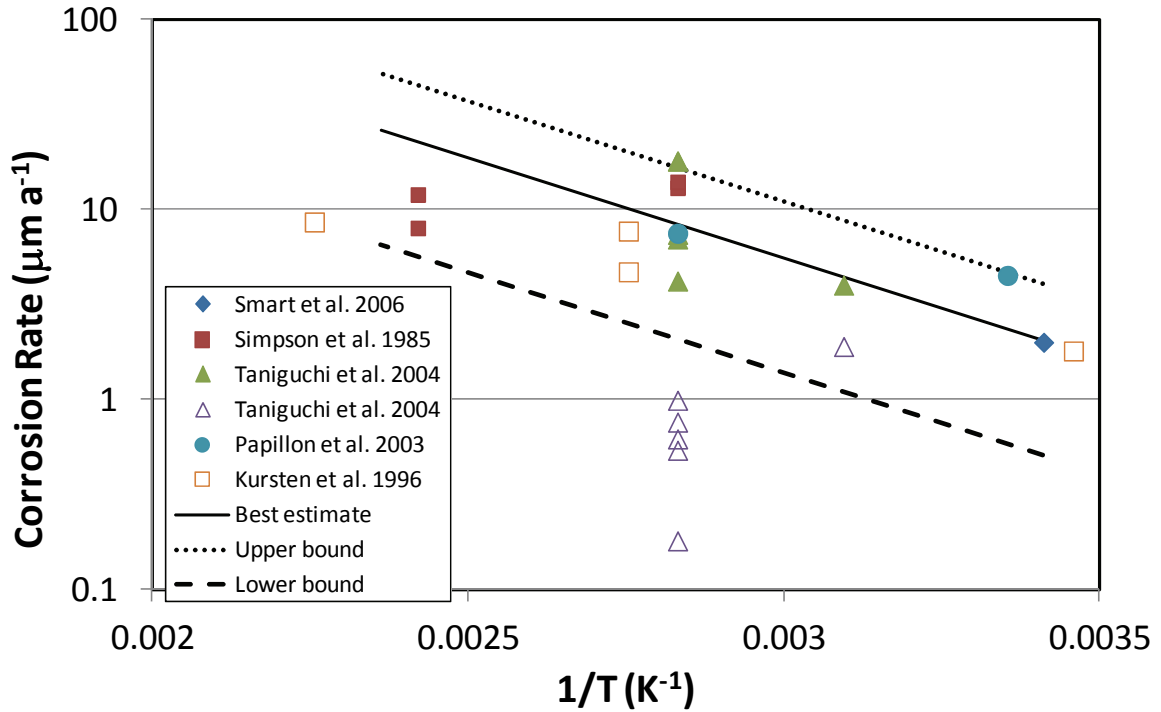


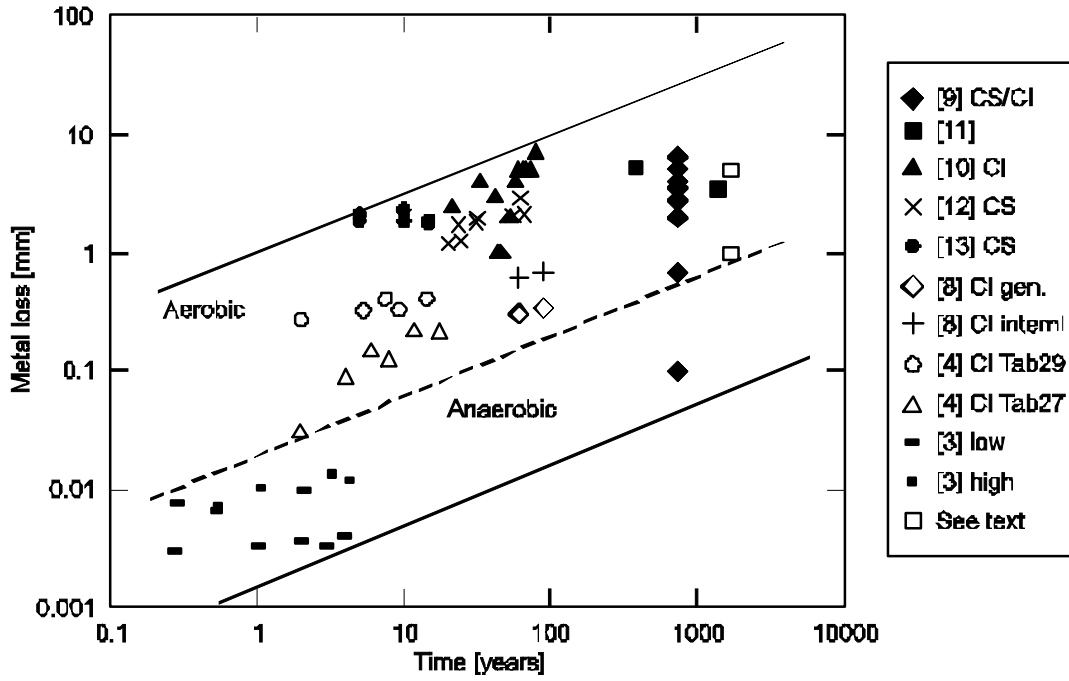
Figure 14: Proposed Best-estimate and Upper and Lower Bound Corrosion Rate Fits for the Corrosion Rate of Carbon Steel During Phase 4

5. UNCERTAINTIES AND CONFIDENCE

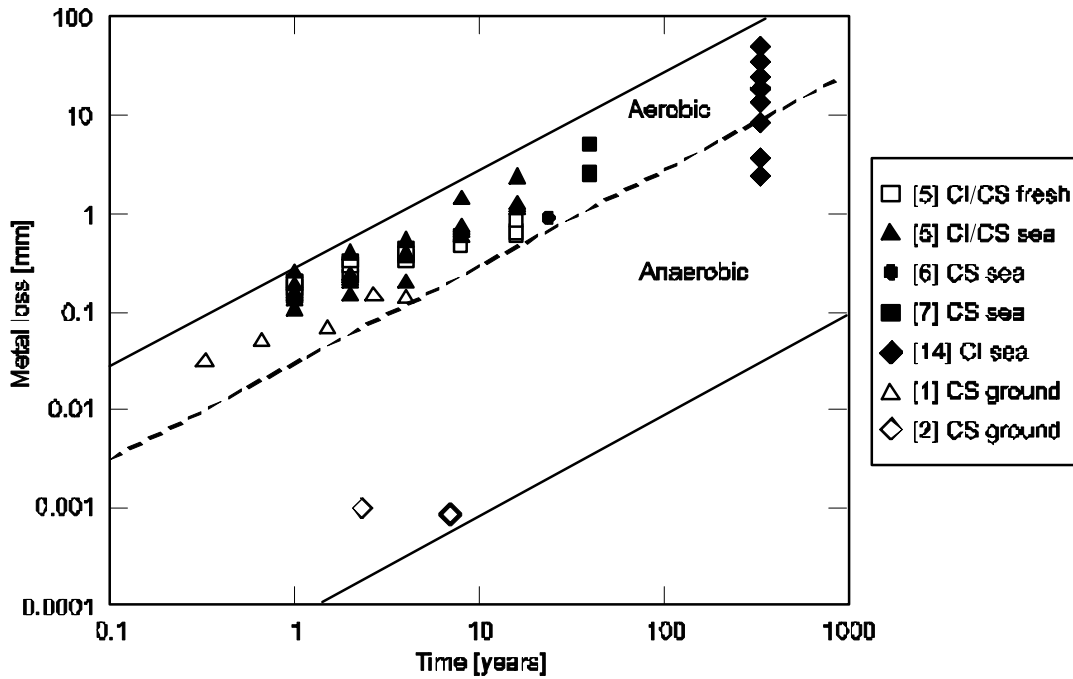
There are a number of uncertainties in the proposed general corrosion model for C-steel UFC, primarily the result of the scatter in the reported data and the relatively few studies under the environmental conditions expected in the repository. Thus, although the database for the unsaturated anaerobic phase is reasonable (albeit limited to a single detailed study), the corresponding database for the unsaturated aerobic phase is poor. Given the relative importance of the oxidation phase (Phase 1), the available data are considered to be adequate. Finally, although there is a reasonable database of corrosion rates in saturated clay under anaerobic conditions (Phase 4), it is unclear whether these rates are appropriate for a Fe_3O_4 -covered surface resulting from pre-exposure to unsaturated anaerobic conditions.

Notwithstanding these uncertainties, the evidence from analogue studies provides some confidence that the range of rates predicted by the model is reasonable. Figure 15 shows a compilation of corrosion depths as a function of time for iron artifacts exposed to soil or aqueous environments (Crossland 2005). The original author has further divided the data into aerobic and anaerobic conditions. It is likely that some of the artifacts exposed to aerobic soil environments were in the unsaturated phase. These artefacts, of course, were exposed at ambient temperature.

Despite the obvious limitations in the use of data from analogues, the ranges of corrosion rates reported are similar to those observed experimentally and which form the basis for the current model. For example, in aerobic soils, Crossland (2005) reports corrosion rates of between $0.6 \mu\text{m}\cdot\text{a}^{-1}$ for artifacts buried up to 1000 a to as high as $1000 \mu\text{m}\cdot\text{a}^{-1}$ for short-term burial. These rates compare with a range for aerobic corrosion in Figure 4 of $8 \mu\text{m}\cdot\text{a}^{-1}$ to $150 \mu\text{m}\cdot\text{a}^{-1}$ for temperatures up to 50°C . Similarly, under anaerobic conditions, Crossland (2005) reports a range of $0.05 \mu\text{m}\cdot\text{a}^{-1}$ to $19 \mu\text{m}\cdot\text{a}^{-1}$, compared with an experimentally measured range at ambient temperature of $1.8 \mu\text{m}\cdot\text{a}^{-1}$ to $4.5 \mu\text{m}\cdot\text{a}^{-1}$ (Figure 11).



(a) Soil



(b) Natural waters

Figure 15: Compilation of Corrosion Rates of Iron and Steel Exposed to Soils and Natural Waters (Crossland 2005)

REFERENCES

- Akiyama, E., K. Matsukado, M. Wang, and K. Tsuzaki. 2010. Evaluation of hydrogen entry into high strength steel under atmospheric corrosion. *Corros. Sci.* 52, 2758-2765.
- Brown, D.A. 1990. *Microbial Water Stress Physiology. Principles and Perspectives*. John Wiley (Chichester, U.K.).
- Casteels, F., G. Dresselaars and H. Tas. 1986. *In Corrosion Behaviour of Container Materials for Geological Disposal of High-Level Waste*. (Editor, B. Haijink), 3-40, Commission of the European Communities Report, EUR 10398 EN.
- Crossland, I. 2005. Long term corrosion of iron and copper. *In ICEM'05: 10th International Conference on Environmental Remediation and Radioactive Waste Management*, September 4–8, 2005 (American Society of Mechanical Engineers, New York, NY), paper ICEM05-1272.
- Debruyne, W. 1990. Corrosion of container materials under clay repository conditions. *In Proceedings of Workshop on Corrosion of Nuclear Fuel Waste Containers*, 1988, February 9 - 10. Winnipeg, MB. (Editor, D.W. Shoesmith). Atomic Energy of Canada Limited Report, AECL-10121, 175-186.
- Desgranges, C., A. Abbas, and A. Terlain. 2003. Model for low temperature oxidation during long term interim storage. *In Prediction of Long Term Corrosion Behaviour in Nuclear Waste Systems*, D. Féron and D.D. Macdonald (eds.), European Federation of Corrosion Publication Number 36 (Maney Publishing, London, UK), Chap 14, pps. 194-207.
- Foet, F. and J.-M. Gras. 2003. Semi-empirical model for carbon steel corrosion in long term geological nuclear waste disposal. *In Prediction of Long Term Corrosion Behaviour in Nuclear Waste Systems*, D. Féron and D.D. Macdonald (eds.), European Federation of Corrosion Publication Number 36 (Maney Publishing, London, UK), Chap 7, pps. 91-102.
- Garisto, F., M. Gobien, E. Kremer, and C. Medri. 2012. Fourth case study: reference data and codes. Nuclear Waste Management Organization Technical Report, NWMO TR-2012-08.
- Gras, J.-M. 1996. Corrosion assessment of metal containers for the geological disposal of HLW. Part 1 : carbon steels, low alloy steels, cast iron. EDF Report No. HT-40/96/002/A, Electricité de France, Moret-sur-Loing, France.
- Guo, R. 2010. Coupled thermal-mechanical modelling of a deep geological repository using the horizontal tunnel placement method in sedimentary rock using CODE_BRIGHT. Nuclear Waste Management Organization Technical Report, NWMO TR-2010-22.
- Honda, A., T. Teshima, K. Tsurudome, H. Ishikawa, Y. Yusa and N. Sasaki. 1991. Effect of compacted bentonite on the corrosion behaviour of carbon steel as geological isolation overpack material. *Mat. Res. Soc. Symp. Proc.* 212, 287-294.

- Johnson, L.H. and F. King. 2008. The effect of the evolution of environmental conditions on the corrosion evolutionary path in a repository for spent fuel and high-level waste in Opalinus Clay. *J. Nucl. Mater.* 379, 9-15.
- King, F. 2005. Overview of the Corrosion Behaviour of Copper and Steel Used Fuel Containers in a Deep Geologic Repository in The Sedimentary Rock of the Michigan Basin. Ontario Power Generation, Nuclear Waste Management Division Report 06819-REP-01300-10101-R00.
- King, F. 2007. Overview of a carbon steel container corrosion model for a deep geological repository in sedimentary rock. Nuclear Waste Management Organization Technical Report, NWMO TR-2007-01.
- King, F. 2008. Corrosion of carbon steel under anaerobic conditions in a repository for SF and HLW in Opalinus Clay. Nagra Technical Report NTB 08-12. Nagra, Wettingen, Switzerland.
- King, F. 2009. Hydrogen effects on carbon steel used fuel containers. Nuclear Waste Management Organization Technical Report, NWMO TR-2009-29.
- King, F. and S. Stroes-Gascoyne. 2000. An assessment of the long-term corrosion behaviour of C-steel and the impact on the redox conditions inside a nuclear fuel waste disposal container. Ontario Power Generation Nuclear Waste Management Division Report No: 06819-REP-01200-10028.
- King, F., M. Kolar and D.W. Shoesmith. 1996. Modelling the effects of porous and semi-permeable layers on corrosion processes. *In* Proc. CORROSION/96, NACE International, Houston, TX, paper no. 380.
- Kursten, B., B. Cornélis, S. Labat, and P. Van Iseghem. 1996. Geological disposal of conditioned high-level and long lived radioactive waste. In situ corrosion experiments. SCK-CEN Report R-3121.
- Larose, S. and R.A. Rapp. 1997. Review of low-temperature oxidation of carbon steels and low-alloy steels for use as high-level radioactive waste package materials. Center for Nuclear Waste Regulatory Analyses report, CNWRA 97-003.
- Leygraf, C. and T.E. Graedel. 2000. Atmospheric Corrosion. Wiley-Interscience, New York.
- Luckner, L., M.Th. van Genuchten, and D.R. Nielsen. 1989. A consistent set of parametric models for the two-phase flow of immiscible fluids in the subsurface, *Water Resources Research* 25, 2187–2193.
- Man, A., and J.B. Martino. 2009. Thermal Hydraulic and Mechanical Properties of Sealing Materials. Nuclear Waste Management Organization Technical Report, NWMO TR-2009-20.
- Newman, R.C., S. Wang, and G. Kwong. 2010. Anaerobic corrosion studies of carbon steel used fuel containers. Nuclear Waste Management Organization Report, NWMO TR-2010-07.

- Papillon, F., M. Jullien, and C. Bataillon. 2003. Carbon steel behaviour in compacted clay: two long term tests for corrosion prediction. In Prediction of Long Term Corrosion Behaviour in Nuclear Waste Systems. European Federation of Corrosion Publication No. 36 (Institute of Materials, Minerals and Mining, London), Chap. 29, p. 439–454.
- Pedersen, K. 2000. Microbial processes in radioactive waste disposal. Swedish Nuclear Fuel and Waste Management Company Report, SKB TR-00-04.
- Rozenfeld, I.L. 1972. Atmospheric Corrosion of Metals. NACE International (Houston, TX),
- Shoesmith, D.W. and F. King. 1999. The effects of gamma radiation on the corrosion of candidate materials for the fabrication of nuclear waste packages. Atomic Energy of Canada Limited Report, AECL-11999.
- Simpson, J.P., R. Schenk, and B. Knecht. 1985. Corrosion rate of unalloyed steels and cast irons in reducing granitic groundwaters and chloride solutions. *Mat. Res. Soc. Symp. Proc.* 50, 429-436.
- Smart, N.R., A.P. Rance, L. Carlson, and L.O. Werme. 2006. Further studies of the anaerobic corrosion of steel in bentonite. *Mat. Res. Soc. Symp. Proc.* 932, 813–820.
- SNC Lavalin. 2011. APM conceptual design and cost estimate update deep geological repository design report crystalline rock environment copper used fuel container. Nuclear Waste Management Organization Technical Report, APM-REP-00440-0001.
- Stroes-Gascoyne, S., C.J. Hamon, C. Kohle and D.A. Dixon. 2006. The effects of dry density and porewater salinity on the physical and microbiological characteristics of highly compacted bentonite. Ontario Power Generation, Nuclear Waste Management Division Report 06819-REP-01200-10016 R00.
- Stroes-Gascoyne, S., C.J. Hamon, D.A. Dixon, C. Kohle and P. Maak. 2007. The effects of dry density and porewater salinity on the physical and microbiological characteristics of highly compacted bentonite. *Mat. Res. Soc. Symp. Proc.* 985, paper 0985-NN13-02.
- Stroes-Gascoyne, S. and C.J. Hamon. 2008. The effect of intermediate dry densities (1.1-1.5 g/cm³) and intermediate porewater salinities (60-90 g NaCl/L) on the culturability of heterotrophic aerobic bacteria in compacted 100% bentonite. Nuclear Waste Management Organization Technical Report NWMO TR-2008-11.
- Taniguchi, N., M. Kawasaki, S. Kawakami, and M. Kubota. 2004. Corrosion behaviour of carbon steel in contact with bentonite under anaerobic condition. In Prediction of Long Term Corrosion in Nuclear Waste Systems. *Proc. 2nd Int. Workshop, Nice, September 2004* (European Federation of Corrosion and Andra), p. 24–34.
- Terlain, A., C. Desgranges, D. Gauvain, D. Féron, A. Galtayries, and P. Marcus. 2001. Oxidation of materials for nuclear waste containers under long term disposal. CORROSION/2001, Paper No. 01119, NACE International (Houston, TX).
- Tsuru, T., Y. Huang, Md.R. Ali, and A. Nishikata. 2005. Hydrogen entry into steel during atmospheric corrosion process. *Corros. Sci.* 47, 2431-2440.

- Turnbull, A. 2009. A review of the possible effects of hydrogen on lifetime of carbon steel nuclear waste canisters. Nagra Technical Report, Nagra NTB 09-04.
- Wersin, P., M. Birgersson, S. Olsson, O. Karnland, and M. Snellman. 2007. Impact of corrosion-derived iron on the bentonite buffer within the KBS-3H disposal concept – the Olkiluoto site as case study. Posiva Oy Report, POSIVA 2007-11.
- Yang, L., R.T. Pabalan, and L. Browning. 2001. Experimental determination of the deliquescence relative humidity and conductivity of multicomponent salt mixtures. *Mat. Res. Soc. Symp. Proc.* 713, 135–142.